Odit, M. A.; Sayanskiy, A. D.; Asadchy, Viktar; Kapitanova, P.; Tretyakov, S. A.; Belov, P. A.

All-dielectric metamirror for independent and asymmetric wave-front control

Published in:
Physical Review B

DOI:
10.1103/PhysRevB.100.205136

Published: 25/11/2019

Document Version
Publisher's PDF, also known as Version of record

Please cite the original version:
Odit, M. A., Sayanskiy, A. D., Asadchy, V., Kapitanova, P., Tretyakov, S. A., & Belov, P. A. (2019). All-dielectric metamirror for independent and asymmetric wave-front control. *Physical Review B*, *100*(20), Article 205136. https://doi.org/10.1103/PhysRevB.100.205136

All-dielectric metamirror for independent and asymmetric wave-front control

M. A. Odit,[1] A. D. Sayanskiy,[1] V. S. Asadchy,[2] P. V. Kapitanova,[1] S. A. Tretyakov,[2] and P. A. Belov[1]
[1]*Department of Physics and Engineering, ITMO University, Russia*
[2]*Department of Electronics and Nanoengineering, Aalto University, Finland*

(Received 18 December 2018; revised manuscript received 4 October 2019; published 25 November 2019)

We report on the design and the numerical and experimental characterization of an all-dielectric reflecting focusing metasurface (metamirror) which does not have a back reflector, but effectively reflects incident waves with the desired reflection phase gradient. The profile of the reflection phase can be tuned independently for both sides of the single-layer subwavelength-thick metamirror by properly selecting dimensions of its dielectric inclusions. Such a feature stems from the bianisotropic omega properties of the inclusions. To demonstrate independent control of the reflection phase, we have designed a metamirror focusing normally incident plane waves at different focal distances being illuminated from the opposite sides. The proposed two-sided metamirror can find applications in antennas, diffraction gratings, and complex holograms. The absence of conducting elements makes it a perfect candidate for optical applications requiring asymmetric wave-front control.

DOI: 10.1103/PhysRevB.100.205136

I. INTRODUCTION

Wave-front engineering is an essential subject of electromagnetics and, in particular, modern nanophotonics. State-of-the-art technologies for communications and sensing require the ultimate miniaturization of optical devices for manipulation of electromagnetic waves [1–7]. One of the routes to attain deeply subwavelength structures for wave-front engineering is the use of plasmonic materials [8–16]. Despite the wide range of applications accessible with plasmonic metasurfaces, they have an inherent drawback, namely, high dissipation loss. Metasurfaces based on dielectric inclusions represent a versatile platform to overcome the problem of plasmonic dissipation loss [17–28]. The inclusions are made of a high-index material and their scattering patterns can be designed by tuning the dielectric Mie-like resonances [29,30].

Most known designs of all-dielectric gradient metasurfaces have symmetric geometry with respect to their plane. This implies equivalence of their electromagnetic response for illuminations from the opposite directions. Breaking this equivalence would open up new possibilities for wave manipulation. Obviously, by introducing an impenetrable metal plate as a part of the metasurface, one can achieve asymmetric reflection from the opposite sides (e.g., by positioning different inclusions at the two sides of the plate). However, such a solution completely disconnects two half spaces and no wave can be transmitted through it in the wide frequency spectrum (up to ultraviolet). The problem of asymmetric reflection without the use of a metal layer is not trivial, but can be solved by using resonant bianisotropic inclusions of omega-shaped topology [21,31–36]. Nevertheless, to the best of our knowledge, *asymmetric and independently designed* wave-front engineering for reflected waves from the opposite sides of a metasurface has not been practically realized.

In this paper, we introduce a design of a gradient metamirror providing asymmetric wave-front transformations being illuminated from the opposite sides (Fig. 1). To demonstrate this property, we implement a focusing reflecting metamirror which provides different focal distances being illuminated from backward [Fig. 1(a)] or forward [Fig. 1(b)] directions. The different response to the opposite directions of illuminations can be tailored independently due to the bianisotropic properties of the metamirror inclusions providing the necessary phase variations of the reflection coefficient. By properly adjusting particles with different dimensions, we can form the required profiles of the reflection phase seen from the two opposite sides of the metamirror. The additional feature of the metamirror presented in this paper is that it is made of a dielectric material only. Therefore, the proposed design can be easily scaled to optical frequencies where conducting loss of metal elements is especially high.

Section II reports the design of an all-dielectric focusing metamirror composed of bianisotropic particles. We demonstrate that such metamirror focuses reflected waves at the designed focal spot and that this behavior is different for different illumination directions. Section III contains the results of experimental verification which was performed in the microwave domain confirming bianisotropic properties of the metamirror. Section IV presents results of the experimental investigation of the metamirror capable of asymmetric reflection and focusing. We demonstrate the possibility of independent tuning of the focusing properties for the same metamirror being illuminated from the opposite directions. Conclusions are presented in Sec. V.

II. ALL-DIELECTRIC METAMIRROR DESIGN AND NUMERICAL VALIDATION

The designed reflecting focusing metasurface (metamirror) consists of a periodic array of dielectric particles (Fig. 1). Each particle has the form of a cylinder with a height H and radius R. There is a notch from one side of the particle with the depth h and radius r (see inset in Fig. 1). Such particle with cylindrical symmetry possesses bianisotropic properties,

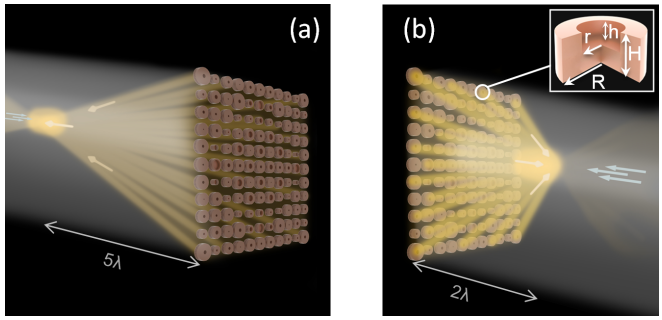

FIG. 1. Metamirror under (a) backward and (b) forward normal illuminations. The inset shows the one-third cutoff of the single bianisotropic particle.

meaning that an external magnetic field induces the electric polarization and an external electric field creates the magnetization in it. A detailed analysis of the bianisotropic properties of such single particle can be found in [32]. The important property of the particle stemming from its bianisotropy is that it can be tuned to ensure an arbitrary phase of reflection from the array (of such particles), maintaining high reflection amplitude close to unity.

We start with the simulation of the reflection properties of the periodic array consisting of identical bianisotropic particles. The reflection coefficient of the infinite array was numerically simulated in the frequency domain solver of the CST STUDIO SUITE 2017. A single particle with imposed periodic boundary conditions was excited with Floquet ports defined in front and behind the unit cell. The reflectarray here exhibits well-known resonant properties of the reflection phase and amplitude [Fig. 2(a)]. Taking into account the axial symmetry of the particle, only one polarization of the normally incident wave was considered. The dimensions of the particle and structure period were originally adjusted so to provide the maximum reflection amplitude at the frequency 10 GHz. This operating frequency can be changed by changing the particle and notch radii as well as their heights [Fig. 2(b)]. The structure period and particle material permittivity were $a = 17$ mm and $\varepsilon = 10$ ($\tan\delta = 0.007$), respectively.

In order to design a flat reflect array, it is necessary to be able to change the reflection phase of the resonating elements from 0 to 2π. For the given particle, this can be done with geometrical tuning. Here the notch and particle radii are

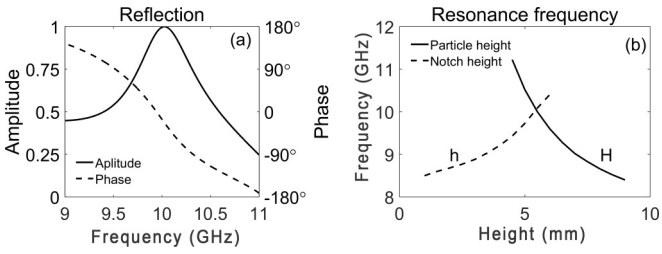

FIG. 2. (a) Reflection coefficient of the infinite periodic array of dielectric bianisotropic particles. Particle dimensions: $R = 7.2$ mm, $r = 5.6$ mm, $H = 7$ mm, $h = 3.5$ mm. Period: $a = 17$ mm. $\varepsilon = 10$. (b) Dependence of the resonance frequency on the particle height H or notch depth h.

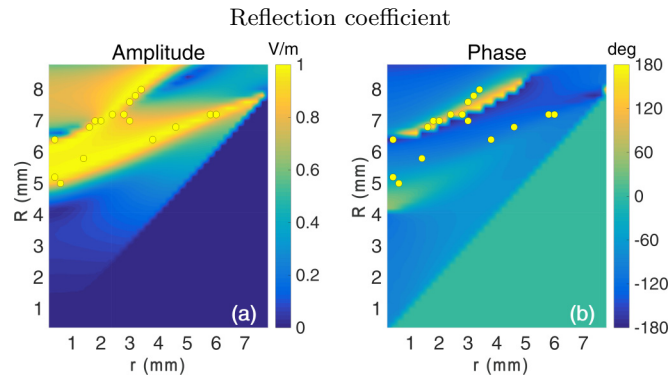

FIG. 3. Simulated (a) amplitude and (b) phase of the reflection coefficient of an infinite array of the bianisotropic particles excited by the normally incident plane wave at the frequency of $f = 10$ GHz. The dots represent selected dimensions of the particles (see Table I).

preferable from the manufacturing point of view. The dependence of the reflection phase of the array on the aforementioned radii has been investigating by numerical simulation of the infinite array with variable parameters. The results of the simulation in terms of the amplitude and phase of the reflection coefficient are presented in Fig. 3 for the forward wave incidence for the given frequency of 10 GHz. The homogeneous triangle area at the bottom of the graphs indicates the nonphysical geometry of the particle ($r > R$). The localized bright region in Fig. 3(a) indicates geometrical sizes with higher reflection amplitude depending on the selected particle geometry (r and R). Figure 3(b) represents the corresponding variations of the reflection phases. It is seen from Fig. 3(b) that the full range of values from $-\pi$ to $+\pi$ can be reached by properly choosing the resonator dimensions.

To design a metamirror that focuses reflected waves, it is necessary to form a parabolic reflection phase profile provided by the elements of the surface [Fig. 4(a)]. The required reflection phase ϕ_{mn} for the particle with the index n in the plane of the metamirror can be calculated from the following equation:

$$\phi_{mn}(r) = \phi_0 + \frac{2\pi}{\lambda}\sqrt{r_{mn}^2 + F^2}, \tag{1}$$

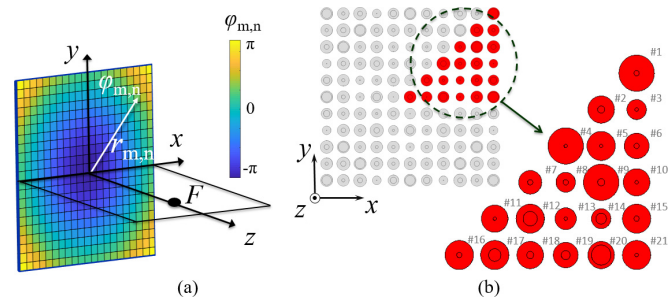

FIG. 4. (a) Distribution of the reflection coefficient phases for the elements of the flat focusing reflecting surface. (b) Finite-size focusing metamirror and enlarged one-eighth part of it showing a unique set of its elements.

TABLE I. Parameters of the metamirror particles.

Particle no.	1	2	3	4	5	6	7	8	9	10	11	12	13	14	15	16	17	18	19	20	21
φ (deg)	−120	−8	120	136	−113	21	−37	51	168	−52	−150	−93	−1	119	−98	170	−170	−112	−19	102	−113
R (mm)	7.2	7.8	7.0	6.8	7.2	7.6	8.0	7.0	7.2	5.2	7.0	5.8	5.8	7.0	6.4	7.2	6.4	6.8	5.0	7.2	7.2
r (mm)	5.8	3.2	2.0	1.6	6.0	3.0	3.4	1.8	2.8	0.4	3.0	1.4	1.4	2.0	3.8	2.8	0.4	4.6	0.6	2.4	6.0

where r_{mn} is the distance from the center of the metamirror to the center of the particle with index mn, λ is the operational wavelength, ϕ_0 is the reflection phase of the central particle, and F is the focal distance.

We limit the number of particles in the metamirror to 11×11 elements, implying that six phase levels provide the appropriate discretization to achieve good focal-spot resolution [37]. The required phases of the reflecting elements were calculated from Eq. (1). From Fig. 3, it is obvious that it is not possible to achieve any arbitrary required reflection phase while keeping near-unity amplitude of the reflection coefficient. The choice should be prioritized between high reflection amplitude and low phase error (defined as the difference between the required and available phase of the particle with given dimensions). In the general case, phases ϕ_i and amplitudes $|\Gamma_i|$ of the reflection coefficients should be selected following the next condition imposed to each element of the designed array:

$$(\phi_{mn} - \phi_i) \to \min, \quad |\Gamma_i| \to \max. \tag{2}$$

In our design, we limit the maximum tolerance of the phase to $\Delta\phi_i \leqslant 10^\circ$, while keeping the value $|\Gamma_i| > 0.8$. To validate the algorithm, we first have designed the metamirror to focus reflected waves at the focal distance $F = 4\lambda$. The particles with corresponding dimensions were selected according to the condition [Eq. (2)] from the available set of simulated dimensions to provide the required parabolic phase profile of the metamirror. The resulted selected values of r and R are shown by yellow dots (see Fig. 3) and listed in Table I. Note that due to the radial symmetry of the metamirror, the number of elements with unique dimensions for the square $N \times N$ array is $(N-1)/2 * [(N-1)/2 - 1] + 1$, which is much less than the total number of the elements in array N^2 [Fig. 4(b)]. The number of unique particles can be even smaller due to the coincidence of the physical dimensions of some of them for given reflection phases.

The finite metamirror structure composed of 11×11 selected elements was numerically simulated with the Integral Solver of the CST STUDIO SUITE 2017. The metamirror was positioned in the xy plane and illuminated normally by a plane electromagnetic wave propagating along the z axis [see Fig. 4(b)]. Open boundaries were defined at all sides of the simulation domain. The simulated amplitude of the x component (the same as that of the incident wave) of the electric field $|E_x|$ is shown in Figs. 5(a) and 5(b). Here we denote as *forward* the direction of illumination when the metamirror is illuminated from the particle notch side. The opposite direction is denoted as *backward*. The scattered field was plotted for the reflected wave, while the total field was plotted for the transmitted wave. All fields are normalized to the incident field measured in free space. The field is plotted at the operational frequency of 10 GHz.

The maximum value of the reflected field occurs at the designed focal spot at the distance of 4λ from the metamirror. The amplitude of the field at the focal point is approximately four times larger than the one of the incident field, indicating remarkable field enhancement in the focal point. In the case of the backward illumination, there is no field focusing at the focal distance. This confirms the asymmetrical behavior of the reflected field in the absence of an opaque conducting plate.

III. EXPERIMENTAL STUDY

In order to verify the numerical results, an experimental prototype of the metamirror was fabricated and its characteristics were measured. We used Eccostock(R) Hic powder as a dielectric material of the particles. This material is characterized by the permittivity of $\varepsilon = 10$ and $\tan\delta = 0.007$ over the microwave frequency range. To form the array of particles, first, their inverse shapes were drilled in a Styrofoam material whose relative permittivity is $\varepsilon_s = 1.1$ and the thickness of the substrate is 20.0 mm. Next, the drilled shapes were filled with the powder.

The experimental study of the metamirror scattering properties was performed in an anechoic chamber. The metamirror was placed horizontally and surrounded with microwave absorbers in order to eliminate edge diffraction (Fig. 6). The incident wave was generated by a broadband horn antenna (the operational range 1–18 GHz) connected to a Rohde & Schwartz ZVB20 vector network analyzer. The antenna was fixed at a distance of 1 m above the metamirror to mimic forward excitation by a quasi-plane wave. For backward excitation, the position of the illuminating antenna was changed to 1 m below the metamirror. The incident field was polarized along the x axis. To measure the distribution of the electric field, an electrically small dipole antenna oriented along the polarization axis was used as a receiving antenna. The dipole was moving within the rectangular 400×600 mm^2 area in the x-z plane starting at the distance of 60 mm from the metamirror. The background excitation signal was subtracted by means of free-space measurement without the metamirror [38]. To reduce the undesired reverberations between the horn and the metamirror, the time gating technique was applied [39]. The measured electric-field magnitudes for the forward and backward illumination directions are shown in Figs. 5(c) and 5(d). It is clearly seen that the metamirror focuses incident field in the case of the forward wave incidence. The measured distance to the focal point where the reflected field has maximum intensity is equal to 4λ. Opposite to the forward illumination, in the case of backward illumination, there is no focusing behavior caused by the metamirror. There is a slight field concentration near the metamirror, which does not correspond to the designed focal distance for forward illumination.

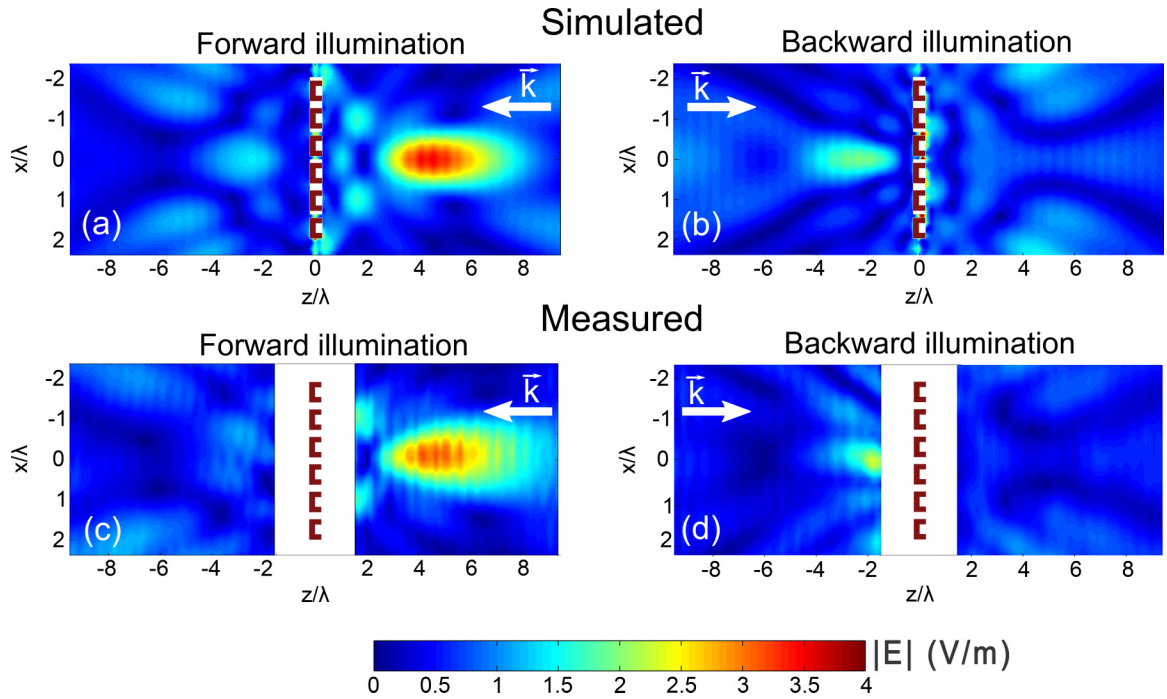

FIG. 5. Electric-field amplitude at the plane orthogonal to the metamirror, which is illuminated from the (a),(c) forward or (b),(d) backward directions at frequency 10 GHz. The scattered field only is plotted on the illumination side, while the total field is plotted for the opposite side.

IV. METAMIRROR WITH INDEPENDENT AND ASYMMETRIC REFLECTION PHASE CONTROL

In the previous section, we have shown the metamirror with asymmetric reflection behavior. Here, we demonstrate that this functionality can be tuned independently for both metamirror sides. For this purpose, we have designed a metamirror that provides focusing of reflected waves at two different focal spots: at 2λ when illuminated in the forward direction and at 5λ when illuminated in the backward direction. In order to strengthen the focusing functionality of the metamirror, we enlarged its aperture by increasing the number of elements up to 17×17 particles. The procedure of the selection of the particles' dimensions was slightly different from the one described in Sec. III. The particles were selected to provide the average deviation between the required and available reflection phases to be less than $\phi_i < 3^\circ$. The average deviation is defined as an average between the phase deviations under forward and backward illumination. In the case where more than one particle satisfied this condition, the one with the highest reflection amplitude $|\Gamma_i|$ was chosen.

All possible reflection coefficient phase and amplitude combinations calculated for the metamirror under study are shown in Fig. 7. The selected particles' dimension values are shown by yellow dots and presented in Table II. The numeration of the particles in the table is similar to the one shown Fig. 4(b). The reflection amplitude is similar to the one in Fig. 4(a). The reflection amplitude is the same for the both illumination directions.

The asymmetrically focusing metamirror was manufactured and measured under the same conditions as described in Sec. III. The measured electric-field amplitude is shown in Fig. 8 in comparison with the results of the numerical

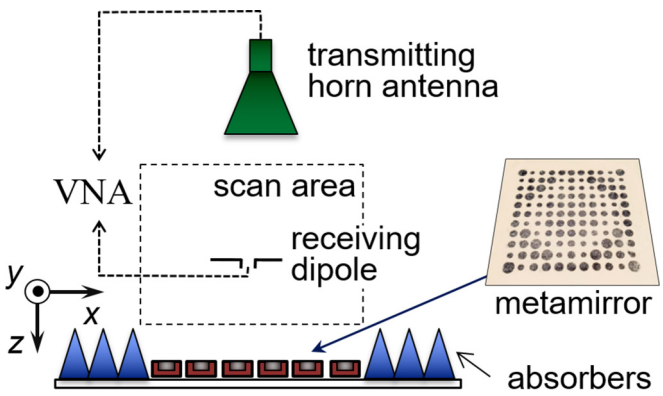

FIG. 6. Experimental setup to measure metamirror properties.

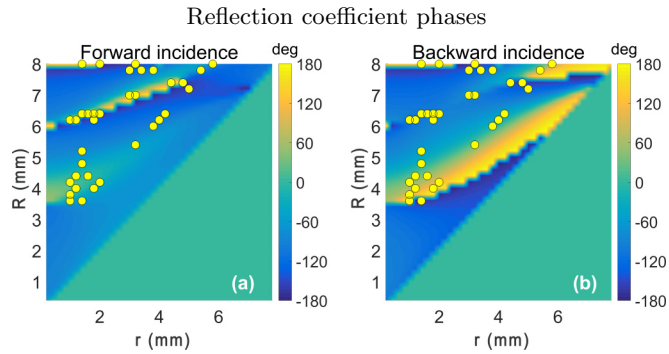

FIG. 7. Reflection coefficient phases for the (a) forward and (b) backward plane-wave incidence on the periodic uniform array. $f = 10$ GHz. The dots represent the selected dimensions of the particles (see Table II).

TABLE II. Parameters of particles comprising the asymmetric focusing metamirror.

Particle no.	1	2	3	4	5	6	7	8	9	10	11	12	13	14	15
φ_{forward} (deg)	−166.8	−104.9	63.7	−32.6	118.8	−88.3	51.6	−116.7	−16.7	170.1	171.8	−59.0	77.3	−95.8	63.7
$\varphi_{\text{backward}}$ (deg)	−65.7	89.3	−77.9	−101.5	−24.9	103.1	−2.9	122.6	−90.5	−47.9	−179.7	−81.4	14.0	154.3	−77.9
R (mm)	3.6	6.4	7.8	6.2	4.2	7.0	4.4	7.4	6.0	3.6	8.0	5.2	4.0	6.4	7.8
r (mm)	1.4	1.6	5.4	4.0	2.0	3.2	1.6	4.4	3.8	1.0	2.0	1.4	1.2	1.8	5.4
	16	17	18	19	20	21	22	23	24	25	26	27	28	29	30
	−106.2	40.8	−162.6	−19.7	−125.8	−16.7	28.1	140.1	−76.9	169.1	−102.2	96.3	−91.5	−132.9	−49.1
	6.8	13.9	−157.0	−46.1	82.0	−90.5	−57.1	−33.6	51.6	176.4	−97.0	11.2	−174.4	−153.8	−113.2
	6.4	4.2	8.0	4.8	6.2	6.0	5.4	4.0	7.0	8.0	7.8	3.8	6.4	7.2	6.4
	1.4	1.0	3.2	1.4	1.0	3.8	3.2	1.8	3.0	1.4	3.8	1.0	2.0	5.0	4.2
	31	32	33	34	35	36	37	38	39	40	41	42	43	44	45
	63.7	−106.2	40.8	−123.8	51.6	−95.8	169.1	−162.1	−90.1	51.4	−106.2	40.8	−137.8	26.2	−117.1
	−77.9	6.8	13.9	−116.6	−2.9	154.3	176.4	−168.0	−143.0	−76.8	6.8	13.9	−129.9	−3.0	152.3
	7.8	6.4	4.2	7.8	4.4	6.4	8.0	7.4	6.2	8.0	6.4	4.2	7.8	4.4	6.2
	5.4	1.4	1.0	3.4	1.6	1.8	1.4	4.8	1.8	5.8	1.4	1.0	3.0	1.2	1.2

simulation. It is clearly seen that the reflected field is focused at the designed focal points when illuminated from the opposite sides. Thus, the reflection phase gradient depends on the direction of the illumination of the metamirror and can be independently designed. The focusing behavior is more pronounced in the case of forward incidence. This can be explained by the more heterogeneous shape of the particle from that side where the notch is present. On the contrary, the opposite side of the particle has a smooth surface without notch leading to less degrees of freedom in changing the reflection phase.

From Fig. 8, one can see that unlike the one-side operational metamirror, there is a remarkable field leakage through the reflecting metamirror. The increased transmission

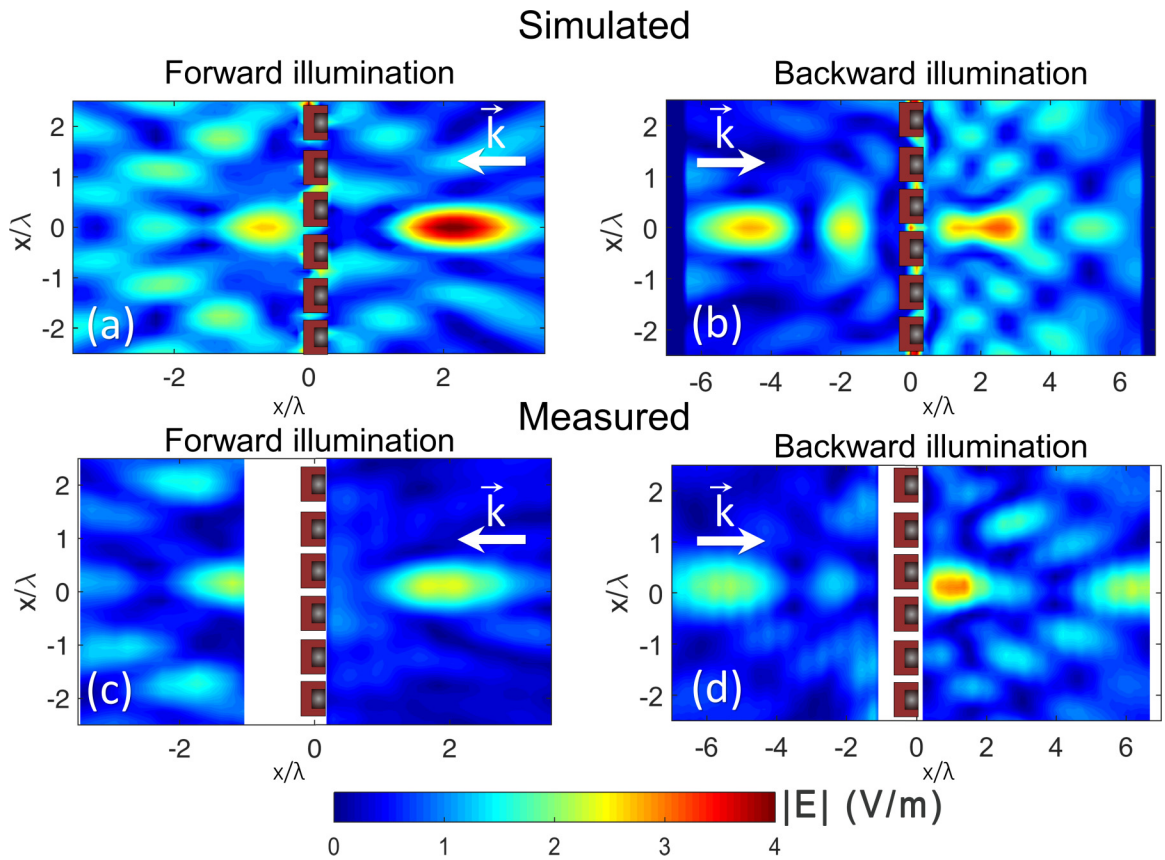

FIG. 8. Electric-field amplitude at the plane orthogonal to the asymmetrically focusing metamirror, which is illuminated from the (a),(c) forward and (b),(d) backward directions at frequency 10 GHz. The scattered field only is plotted on the illumination side, while the total field is plotted for the opposite side.

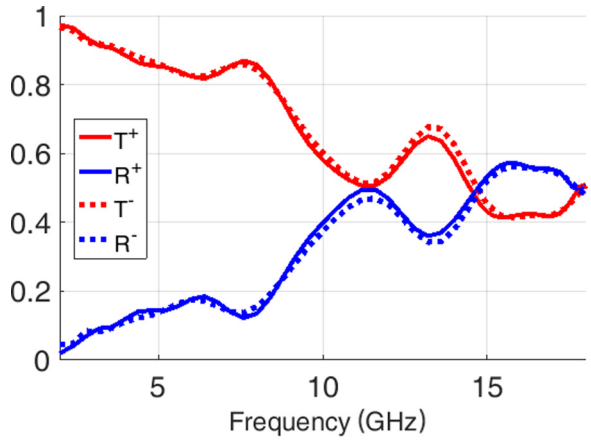

FIG. 9. Reflectance (R) and transmittance (T) of the asymmetric metamirror under forward ($^+$) or backward ($^-$) illumination.

is caused by the lower reflection amplitudes and increased difference between the required and available reflection phases [see Eq. (2)]. This is the price of the asymmetrical functionality of the metamirror. Nevertheless, the field amplification in the focal spot varies from 2.5 for the backward illumination to 3.5 for the forward one. There is also the additional focusing effect of the transmitted wave which can be harmful for some applications. It can be explained by the similar parabolic phase profile of the transmitted wave phase. This effect is comparable with the focusing of the reflected wave and more pronounced than for the one-sided metamirror. Nevertheless, the focusing of the transmitted wave can be reduced if required by further optimizing the structure. This is possible by proper selection of the reflecting particle dimensions and by changing weights between the higher reflection amplitude and more precise reflection phase.

As it was mentioned, the remarkable feature of the presented metamirror is the absence of a conducting ground plane. This property is important in the case where one needs to have a semitransparent surface transmitting electromagnetic energy at the frequencies other than operating. In order to evaluate the opacity of the metamirror, we calculated the integral power flow over the two surfaces in front and behind the metamirror. The surface area is equal to the metamirror aperture. The faces are placed at $z = H/2$ and $z = -H/2$ positions, i.e., they touch the metamirror particles at the top and bottom. The power value was normalized to the one in a free space passing through the same area. The calculation results for the forward and backward illuminations are presented in Fig. 9. As one can see, the structure remains transparent below the resonance band and the reflection increases only around the resonance frequency and above. Although reflection remains relatively high above the resonance, half of the energy passes through the metasurface that would be impossible in the case of a conventional reflectarray.

V. CONCLUSION

An asymmetric all-dielectric focusing metamirror composed of bianisotropic dielectric particles was studied numerically and experimentally. It was demonstrated that such metamirror can strongly reflect incident waves, focusing them at a designed focal point, and that this behavior has an asymmetric nature due to the bianisotropy of the metamirror elements. Such functionality can be used in the optical domain to design all-dielectric metamirrors to control the reflection phase profile. One should note that focusing properties can be further improved by modifying the dielectric resonator shape and improving the manufacturing process.

It was also numerically and experimentally verified that a metamirror based on bianisotropic particles can be tuned to exhibit different and independent reflection properties being illuminated from the opposite sides. This opens up a possibility to independently control the reflection phase profile of a single-layer metamirror being illuminated from opposite directions. Moreover, the metamirror does not contain conducting elements, which makes it a perfect candidate for dielectric photonic structures intended for low-loss light manipulation.

ACKNOWLEDGMENTS

This research was supported by RFBR (Grant No. 18-37-00486). V.A. acknowledge support of the Academy of Finland (Project No. 287894). This research was supported by the Ministry of Education and Science of the Russian Federation (Zadanie No. 3.2465.2017/4.6). This work was supported in part by the Finnish Foundation for Technology Promotion.

[1] L. Novotny and B. Hecht, *Principles of Nano-Optics* (Cambridge University Press, New York, 2006).
[2] S. A. Maier, *Plasmonics: Fundamentals and Applications* (Springer Science & Business Media, New York, 2007).
[3] A. V. Zayats, I. I. Smolyaninov, and A. A. Maradudin, Phys. Rep. **408**, 131 (2005).
[4] S. Lal, S. Link, and N. J. Halas, Nat. Photon. **1**, 641 (2007).
[5] H. A. Atwater and A. Polman, Nat. Mater. **9**, 205 (2010).
[6] A. Krasnok, S. Li, S. Lepeshov, R. Savelev, D. G. Baranov, and A. Alú, Phys. Rev. Appl. **9**, 014015 (2018).
[7] S. Lepeshov, A. Gorodetsky, A. Krasnok, N. Toropov, T. A. Vartanyan, P. Belov, A. Alú, and E. U. Rafailov, Sci. Rep. **8**, 6624 (2018).
[8] N. Yu, P. Genevet, M. A. Kats, F. Aieta, J.-P. Tetienne, F. Capasso, and Z. Gaburro, Science **334**, 333 (2011).
[9] S. Sun, K.-Y. Yang, C.-M. Wang, T.-K. Juan, W. T. Chen, C. Y. Liao, Q. He, S. Xiao, W.-T. Kung, G.-Y. Guo, L. Zhou, and D. P. Tsai, Nano Lett. **12**, 6223 (2012).
[10] F. Monticone, N. M. Estakhri, and A. Alù, Phys. Rev. Lett. **110**, 203903 (2013).
[11] A. Pors and S. I. Bozhevolnyi, Opt. Exp. **21**, 27438 (2013).
[12] M. Kim, A. M. H. Wong, and G. V. Eleftheriades, Phys. Rev. X **4**, 041042 (2014).
[13] Z. Li, L. Huang, K. Lu, Y. Sun, and L. Min, Appl. Phys. Exp. **7**, 112001 (2014).

[14] Y. Z. Ho, B. H. Cheng, W.-L. Hsu, C.-M. Wang, and D. P. Tsai, Appl. Phys. Exp. **9**, 072502 (2016).
[15] A. Epstein and G. V. Eleftheriades, J. Opt. Soc. Am. B **33**, A31 (2016).
[16] V. S. Asadchy, A. Wickberg, A. Díaz-Rubio, and M. Wegener, ACS Photon. **4**, 1264 (2017).
[17] D. Lin, P. Fan, E. Hasman, and M. L. Brongersma, Science **345**, 298 (2014).
[18] M. L. Brongersma, Y. Cui, and S. Fan, Nat. Mater. **13**, 451 (2014).
[19] M. Decker, I. Staude, M. Falkner, J. Dominguez, D. N. Neshev, I. Brener, T. Pertsch, and Y. S. Kivshar, Adv. Opt. Mater. **3**, 813 (2015).
[20] S. Jahani and Z. Jacob, Nat. Nanotechnol. **11**, 23 (2016).
[21] V. Asadchy, M. Albooyeh, and S. Tretyakov, J. Opt. Soc. Am. B **33**, A16 (2016).
[22] A. I. Kuznetsov, A. E. Miroshnichenko, M. L. Brongersma, Y. S. Kivshar, and B. Luk-yanchuk, Science **354**, aag2472 (2016).
[23] E. Khaidarov, H. Hao, R. Paniagua-Domínguez, Y. F. Yu, Y. H. Fu, V. Valuckas, S. L. K. Yap, Y. T. Toh, J. S. K. Ng, and A. I. Kuznetsov, Nano Lett. **17**, 6267 (2017).
[24] P. Genevet, F. Capasso, F. Aieta, M. Khorasaninejad, and R. Devlin, Optica **4**, 139 (2017).
[25] W. Liu and A. E. Miroshnichenko, ACS Photon. **5**, 1733 (2018).
[26] R. Paniagua-Domínguez, Y. F. Yu, E. Khaidarov, S. Choi, V. Leong, R. M. Bakker, X. Liang, Y. H. Fu, V. Valuckas, L. A. Krivitsky, and A. I. Kuznetsov, Nano Lett. **18**, 2124 (2018).
[27] A. Sayanskiy, M. Danaeifar, P. Kapitanova, and A. E. Miroshnichenko, Adv. Opt. Mater. **6**, 1800302 (2018).
[28] L. Wang, S. Kruk, K. Koshelev, I. Kravchenko, B. Luther-Davies, and Y. Kivshar, Nano Lett. **18**, 3978 (2018).
[29] P. E. Landreman, H. Chalabi, J. Park, and M. L. Brongersma, Opt. Express **24**, 29760 (2016).
[30] S. Lepeshov and Y. Kivshar, ACS Photon. **5**, 2888 (2018).
[31] Y. Ra'di, V. S. Asadchy, and S. A. Tretyakov, IEEE Trans. Antennas Propag. **62**, 3749 (2014).
[32] R. Alaee, M. Albooyeh, A. Rahimzadegan, M. S. Mirmoosa, Y. S. Kivshar, and C. Rockstuhl, Phys. Rev. B **92**, 245130 (2015).
[33] V. S. Asadchy, Y. Ra'di, J. Vehmas, and S. A. Tretyakov, Phys. Rev. Lett. **114**, 095503 (2015).
[34] M. Yazdi, M. Albooyeh, R. Alaee, V. Asadchy, N. Komjani, C. Rockstuhl, C. R. Simovski, and S. Tretyakov, IEEE Trans. Antennas Propag. **63**, 3004 (2015).
[35] M. Odit, P. Kapitanova, P. Belov, R. Alaee, C. Rockstuhl, and Y. S. Kivshar, Appl. Phys. Lett. **108**, 221903 (2016).
[36] V. S. Asadchy, A. Díaz-Rubio, and S. A. Tretyakov, Nanophotonics **7**, 1069 (2018).
[37] C. Saeidi and D. van der Weide, Appl. Phys. Lett. **106**, 113110 (2015).
[38] C. Larsson, C. Sohl, M. Gustafsson, and G. Kristensson in *Proc. of Nordic Conf. on Radio Science and Communications* (2008), pp. 127–129.
[39] R. De Porrata-Doria i Yague, A. B. Ibars, and L. F. Martinez, IEEE Trans. Instrum. Meas. **47**, 930 (1998).